Flow and Heat Transfer Measurements of Film Injectant from a Row of Holes with Compound Angle Orientations

Bumsoo Han, Dong Kee Sohn, Joon Sik Lee*

School of Mechanical & Aerospace Engineering, Seoul National University, Seoul 151-742, Korea

An experiment has been conducted on the flow and heat transfer characteristics of film coolant injected from a row of five holes with compound angle orientations of 35° inclination angle and 45° orientation angle. The Reynolds number number based on the mainstream velocity and injection hole diameter 3.58×10^4. Three-dimensional velocity, film cooling effectiveness and heat transfer coefficient data are presented at three different mass flux ratios of 0.5, 1.0 and 2.0. Flow entrainment has been found between the vortices generated by adjacent injectants. The injectant with compound angle orientation entrains not only the mainstream boundary layer flow but also the adjacent injectant. Because of the flow entrainment, the injectant. With compound angle orientation is characterized by a single vortex while two bound vortices are usually observed in the case of simple angle injection. The strength of the secondary flow depends strongly on the mass flux ratio, which shows significant influence on the film cooling effectiveness and heat transfer coefficient.

Key Words: Film Cooling, Compound Angle Orientations, Mass Flux Ratio, Film Cooling Effectiveness, Heat Transfer Coefficient

Nomenclature

D : Injection hole diameter [m]
h : Heat transfer coefficient [W/m²K]
L : Injection hole length [m]
M : Mass flux ratio, $\rho_j U_j/\rho_\infty U_\infty$
q : Heat flux [W/m²]
Re_D: Reynolds number, $U_\infty D/\nu$
S : Pitch between adjacent holes [m]
T : Temperature [℃]
U : Velocity [m/s]
x : Streamwise coordinate
y : Coordinate normal to the surface
z : Spanwise coordinate
α : Inclination angle
β : Orientation angle
η : Film cooling effectiveness
ν : Kinematic viscosity [m²/s]
ρ : Density

Subscripts

aw : Adiabatic wall
j : Injectant
0 : Condition without film cooling
f : Condition with film cooling
w : Wall
∞ : Mainstream

* Corresponding Author,
E-mail : jslee@gong.snu.ac.kr
TEL : +82-2-880-7117; **FAX** : +82-2-883-0179
School of Mechanical & Aerospace Engineering, Seoul National University, Seoul 151-742, Korea. (Manuscript **Received** July 3, 2001; **Revised** May 29, 2002)

1. Introduction

Film cooling technique is one of the widely used cooling methods for blades of high efficiency gas turbines. Various types of film hole arrangements have been surveyed to obtain high film cooling effectiveness. Recently, injection with compound angle orientation is suggested because it provides more uniform film coverage. The compound angle orientation can be identified by two injection angles, the inclination angle α and the orientation angle β as depicted in Fig. 1. The inclination angle is defined as the angle between

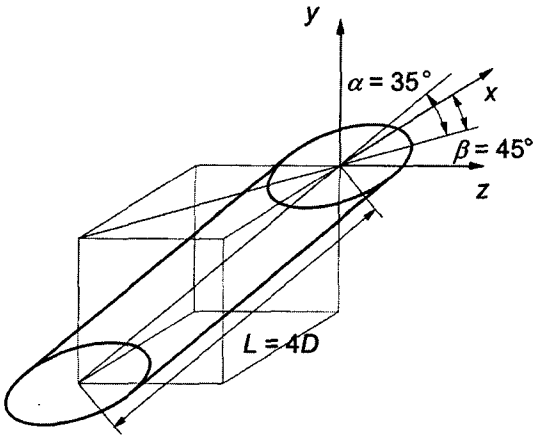

(a) Injection hole geometry

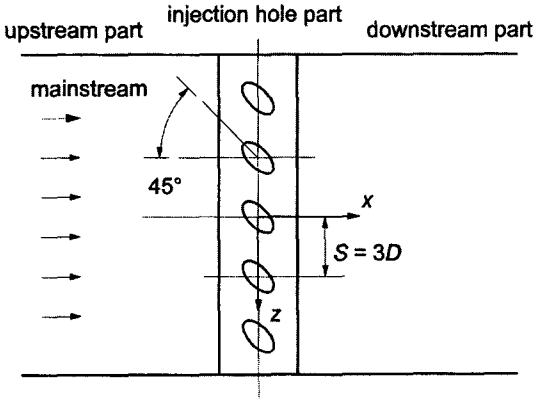

(b) Test plate

Fig. 1 Injection hole geometry and coordinate system

the injection vector and its projection on x-z plane, and the orientation angle as the angle between the streamwise direction and projection of the injection vector on the x-z plane. Injection with compound angle orientation has lateral momentum that causes more uniform film coverage in the spanwise direction than with simple angle injection at a same mass flux ratio. Although many experimental studies have been carried out on simple angle injection, only a few studies were reported on film cooling with compound angle injection.

Ligrani et al. (1992, 1994a, 1994b) reported that the compound angle injection configuration provided significantly improved film cooling protection compared to the simple angle one for the same spanwise hole spacing, normalized streamwise location and mass flux ratio. In the experimental studies by Ligrani and Lee (1996a, 1996b) they surveyed film cooling from both a single row and two staggered rows of compound angle holes at high mass flux ratios. Ekkad et al. (1997a, 1997b) showed that both film effectiveness and heat transfer coefficient increased as the orientation angle increased from 0° to 90°. They also observed that the effectiveness was much higher in the case of compound angle injection at large momentum ratios.

According to Sen et al. (1996) and Schmidt et al. (1996) who provided heat transfer and effectiveness results for compound angle film cooling with hole shape variation, the compound angle film cooling had greater film cooling effectiveness and increased heat transfer level at large mass flux ratio. Lee et al. (1997) measured three-dimensional velocity field of single jet with compound angle orientation, and found that as the orientation angle increased, a pair of counter-rotating vortices turned to a single strong one, and the aerodynamic loss is produced within the jet region.

More recently, Ahn et al. (2001a, 2001b) investigated film cooling performance from two rows of holes with opposite orientation angles, and reported detailed adiabatic film cooling effectiveness and heat transfer coefficient distributions measured using a TLC (Thermochromic Liquid Crystal) technique. In their study, they evaluated film cooling performance in terms of heat flux ratio.

Most previous studies have separately surveyed surface heat transfer or fluid dynamics behaviors. For a clear understanding, however, it is essential to provide both flow and heat transfer data together, to analyze the film cooling performance with compound angle orientation, and to pursue the improvement of film cooling performance.

The present film cooling system consists of a row of five holes with 35° inclination angle and 45° orientation angle. Presented are three-dimensional velocity, adiabatic wall temperature, and heat transfer coefficient date for mass flux ratio of 0.5, 1.0 and 2.0.

2. Experimental Apparatus and Procedure

Figure 2 shows schematic of experimental set-up. The wind tunnel is an open-type subsonic one with 6 : 1 contraction ratio. The exit of the wind tunnel is followed by the test section, which is of a rectangular duct of 690 mm wide, 460 mm high and 1500 mm long. At a mainstream velocity of 15 m/s, the spatial uniformity of streamwise mean velocity is 0.4% and the turbulent intensity is less than 0.2%. A trip wire is attached at the nozzle exit to provide a turbulent boundary layer flow over the test plate.

The air supplied from a blower enters plenum chamber through an orifice which is installed to measure the injectant flow rate. A heat exchanger is placed in the plenum chamber to uniformly heat the injected air. Injection holes are located 465 mm downstream from the trip wire and the injection hole diameter, D is 30 mm. Five injection holes are located at $z/D=-6$, -3, 0, 3 and 6. The ratio of hole length-to-diameter L/D is 4, The actual gas turbine has the ratio in the range of 1.5~8.

A five-hole Pitot tube is used to measure the three-dimensional velocity field. The pressure at each hole of the Pitot tube is transformed to DC voltage by a pressure transducer and a scanni-valve. Th electric signals are sampled by a digital multimeter and transferred into the computer.

The three-dimensional traverse system is used to move probe with 20 μm resolution. In using five-hole Pitot tube, probe is roughly aligned within $\pm 5°$ using stepping motor. Then yaw-pitch calibration data are used to determine three-dimensional velocity. The stepping motor and traverse system are controlled by the personal computer.

A heating plate is used to determine heat transfer coefficient. The heating plate is of 30 μm-thickness stainless steel foil bonded on the polycarbonate sheet (Lexan) of 3 mm thickness. The bottom side of polycarbonate plate is insulated with styrofoam. The spanwise ends of the stainless steel foil are connected to AC current source by copper bus bars. This surface is regarded as a constant heat flux wall when heated and as an adiabatic wall when unheated. The heating plate is place 495 mm downstream from the trip wire. Wall temperatures are measured using 109 thermocouples, which are attached between stainless steel foil and polycarbonate sheet. The electro-

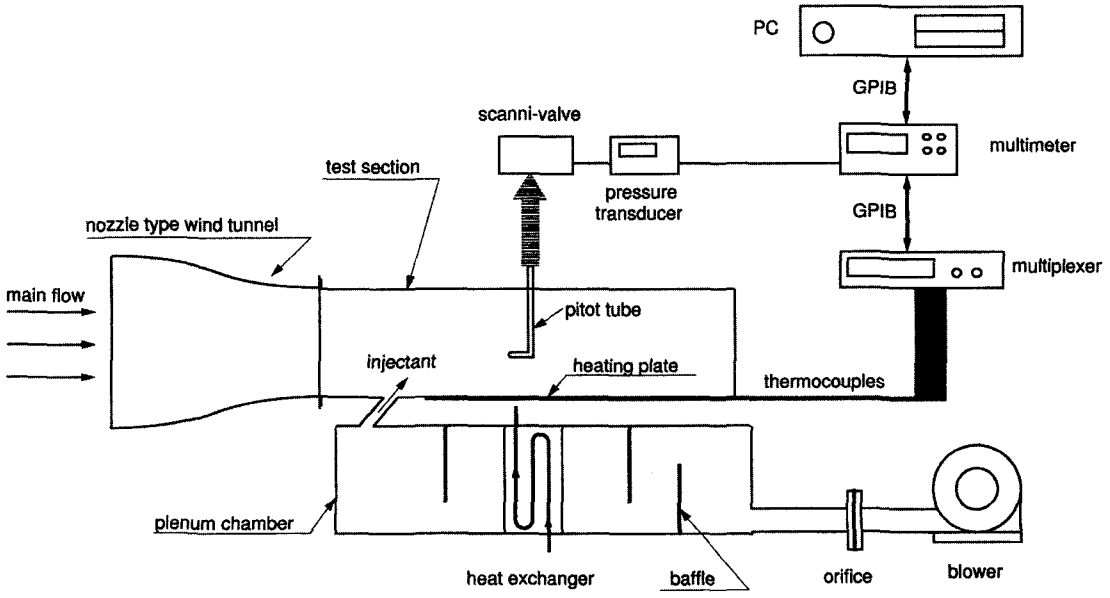

Fig. 2 Schematic diagram of experimental set-up

motive force signals from the thermocouples transmitted through a multiplexer to a digital multimeter, which is interfaced with personal computer by a GPIB.

During all experiments, mainstream velocity, U_∞ is maintained 15 m/s. The displacement and momentum boundary layer thicknesses are 1.90 mm and 1.46 mm, respectively, at the center of the injection hole. The Reynolds number based on the mainstream velocity and injection hole diameter, $Re_D=U_\infty D/\nu$, is 3.58×10^4. The injectant velocity is changed to be $M=0.5$, 1.0 and 2.0 where M is the ratio of injectant mass flux to mainstream mass flux. The temperature difference between mainstream and injectant is controlled to within ±0.2℃ during the flow measurement. The measurement is carried out in the y-z plane at $x/D=5$ and 10 with an interval of $D/5$ in both y and z directions.

Both the film effectiveness and the heat transfer coefficient are measured. In the effectiveness measurement, the test plate is unheated, on the other hand, the injectant is heated to get higher temperature than mainstream temperature by 20℃ using the heat exchanger in the plenum chamber. The density ratio between injectant and mainstream is 0.93. The film cooling effectiveness η is defined as

$$\eta=\frac{T_{aw}-T_\infty}{T_j-T_\infty} \tag{1}$$

The adiabatic wall temperature T_{aw} is directly measured from the unheated test plate.

In the heat transfer coefficient measurement, the injectant and mainstream are maintained at the same temperatures, on the other hand, the test plate is electrically heated. According to Eckert (1984), the relationship the heat flux and the heat transfer coefficient with film cooling can be defined as

$$q_f=h_f(T_{aw}-T_w) \tag{2}$$

where T_w, h_f and q_f denote the wall temperature, heat tansfer coefficient and heat flux with film cooling, respectively. Another way of defining the heat transfer coefficient is

$$q_f=h(T_\infty-T_w) \tag{3}$$

Dividing both sides of Eq. (3) by Eq. (2) and rearranging, it follows that

$$\frac{h}{h_f}=1-\eta\frac{T_j-T_\infty}{T_w-T_\infty} \tag{4}$$

As can be seen in Eq. (4), when the injectant and the mainstream temperatures are the same, h_f becomes identical with h. The heat transfer coefficient is thus obtained as

$$h=\frac{q_f}{T_w-T_\infty} \tag{5}$$

The uncertainty of the adiabatic wall temperature can be caused by the aerodynamic heating, and conduction radiation losses. To compensate the heat loss of heating plate, one-dimensional energy balance is used according to Mick and Mayle (1988). The error due to spanwise heat conduction through the stainless foil and base plate is estimated to less then 3.5% and hence no correction is made.

The uncertainty analysis is evaluated on 20 to 1 odds (95% confidence level). All the uncertainty values are evaluated from the method of single-sample experiments proposed by Kline and McClintock (1953). The uncertainty of the adiabatic film cooling effectiveness is 5.9% at a typical η value of 0.2. The uncertainty value of the adiabatic film cooling effectiveness is getting larger as the difference between the mainstream and the boundary layer temperatures becomes smaller. For example, the uncertainty value increases up to 29.5% at $\eta=0.05$. In the same manner, the uncertainty of the heat transfer coefficient is estimated as 6.8%.

3. Results and Discussion

3.1 Three dimensional velocity fields

Film coolant flow from holes with compound angle orientations shows strikingly different structure from that with a simple angle orientation. It loses its symmetry and only one-directional vortex structure is observed in the downstream region, while the coolant flow with simple angle orientation is characterized by a counter-rotating vortex pair.

Streamwise mean velocity contours in the cross-

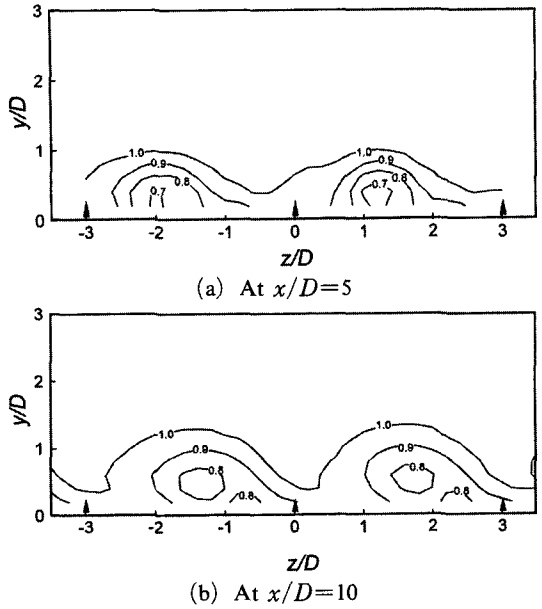

(a) At $x/D=5$

(b) At $x/D=10$

Fig. 3 Streamwise velocity contour at $M=1.0$

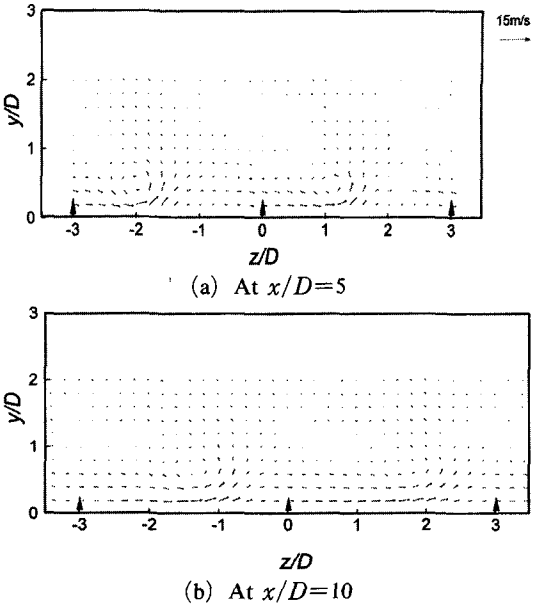

(a) At $x/D=5$

(b) At $x/D=10$

Fig. 4 Secondary flow velocity vectors at $M=1.0$

sectional planes are presented in Fig. 3 when the mass flus ratio M is unity. Because of periodic characteristics, plotted are representatively the contours of film flows originated from two holes located at $z/D=0$ and 3, as marked by arrows. At $M=1.0$, the injected jets lift off from the wall but the trajectory is closer to the wall comparing to the simple angle injection. Injectant momentum with compound angle divided into normal and lateral components, while the injectant with simple angle has only a stronger normal momentum component. The trajectory is deflected to the z-direction due to lateral momentum of the injectants. The deflection is getting wider as flow proceeds downstream. For example, the injectant trajectory is deflected by about $1.0D$ at $x/D=5$ (see Fig. 3(a)), and by about $1.7D$ at $x/D=10$ (see Fig. 3(b)) in the spanwise direction.

Figure 4 shows the secondary flow velocity vectors at $M=1.0$. It is clearly seen that a single vortex structure is associated with each injectant accumulation. An interesting flow behavior is that flow entrainment occurs from left to right between the vortices. The injectant with compound angle orientation entrains not only the mainstream boundary layer flow but also the adjacent injectant. Due to the entrainment between injectants, the film cooling effectiveness is expected to be more uniform than that with a simple angle orientation where significant non-uniformity in the film cooling effectiveness is observed between a region occupied by the injectants and the other region which is not covered by the injectants. In the downstream region, as can be seen in Fig. 4(b), the vortex strength becomes weaker.

Figure 5 and 6 show streamwise mean velocity contours and secondary flow velocity vectors, respectively, at $M=2.0$. In this case, the injectants lift further off from the wall than in the case of $M=1.0$ simply because of the stronger vertical momentum. Velocity deficit at the right lower part of each injectant shown in Fig. 5(a) is due to the wake flow, resulting from lift-off of injectants. A vigorous mixing which causes a rapid diffusion of injectant occurs in opposition to that at $M=1.0$ shown in Fig. 5(b).

In Fig. 6(a), two vortex centers of each injectant are observed and the secondary flow is much stronger than that at $M=1.0$. One vortex is formed within the injectant, and the other is a jet-wake vortex that appears in the wake generated due to lift-off of the injectant as observed by Honami et al. (1994). One vortex center is found

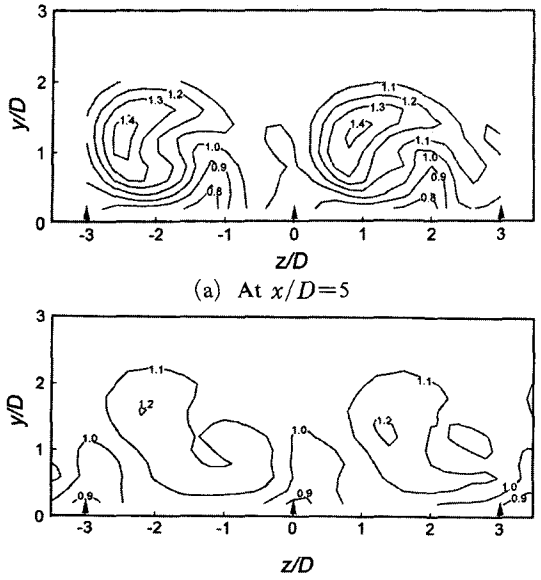

(a) At $x/D=5$

(b) At $x/D=10$

Fig. 5 Streamwise velocity contour at $M=2.0$

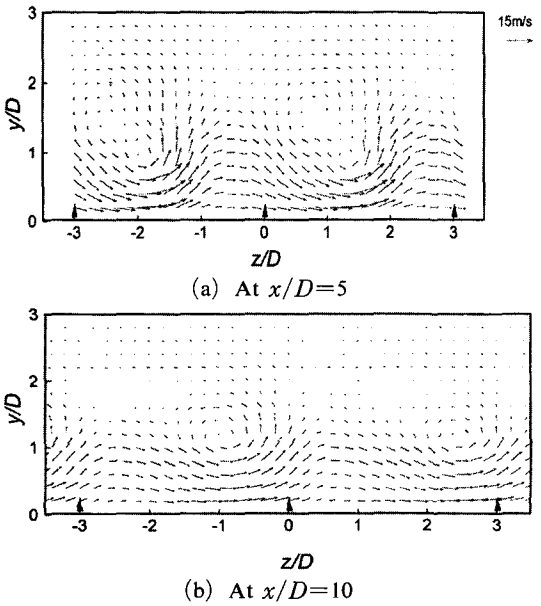

(a) At $x/D=5$

(b) At $x/D=10$

Fig. 6 Secondary flow velocity vectors at $M=2.0$

at $y/D=1.7$ and $z/D=0.8$, the other at $y/D=1.0$ and $z/D=1.3$. The upper one is formed from mainstream creeping over the injectant and the bottom one from the wake caused by the injectant which acts like a blunt body against the mainstream. In the downstream region, two vortices merge into one as flow mixing proceeds (see Fig. 6(b)), however, flow entrainment between adjacent injectants is still strong.

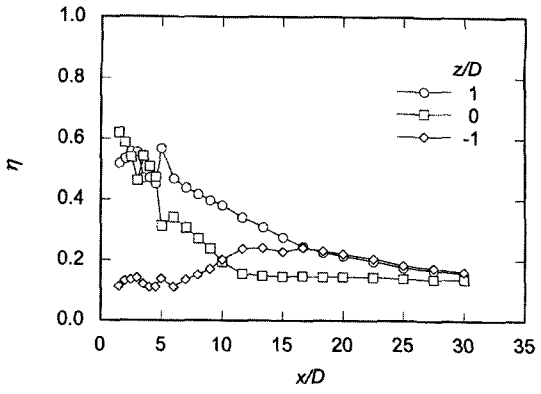

(a) Streamwise distribution

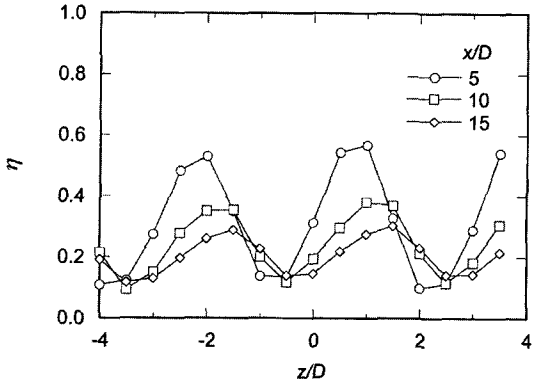

(b) Spanwise distribution

Fig. 7 Local film cooling effectiveness at $M=0.5$

3.2 Film cooling effectiveness

Distributions of the local film cooling effectiveness at $M=0.5$ are presented in Fig. 7. Figure 7(a) shows the streamwise distribution along the lines of $z/D=-1$, 0 and 1. Along the $z/D=0$ line, the effectiveness has a pretty high value of 0.62 near the injectant exit and then decreases rapidly until it reaches an asymptotic value of 0.14 beyond $x/D=12$. Along the $z/D=1$ line, a peak near $x/D=5$ and then gradually decreases. This peak occurs because the injectant originated from the hole at $z/D=0$ is deflected and crosses the $z/D=1$ line at $x/D=5$. Along the $z/D=-1$ line, the effectiveness is as 0.11 for about $x/D<5$ because this region is a blind region which is not covered by the injectant. After $x/D=5$, it gradually increases up to about $x/D=12$

and then decreases thereafter. The increase from $x/D=5$ results from the fact that the injectant originated from the hole at $z/D=-3$ reaches $z/D=-1$ at $x/D=12$.

Figure 7(b) shows the spanwise distribution of the film cooling effectiveness at $x/D=5$, 10 and 15. Two peaks at each streamwise location are identical to the centers of injectant trajectories and are shifting to right in the downstream region. The local maximum at $x/D=5$ occurs at $z/D=-2$ and 1. These peak points migrate to the z-direction as moving downstream, because of the lateral momentum of injectants.

The effectiveness distribution along the $z/D=0$ line for $M=1.0$ (see Fig. 8(a)) shows strikingly different behavior from that at $M=0.5$ (see Fig. 7 (a)). The effectiveness is much lower near the exit compared to that at $M=0.5$ because the injectant has a stronger lateral momentum so that it is deflected and deviated from the $z/D=0$ line immediately after injected. Then, the effectiveness gradually increases to have its maximum at about $x/D=15$. When $M=1.0$, the injectant from the hole at $z/D=-1$ has strong enough momentum to maintain its structure crossing the $z/D=0$ line at $x/D=15$. This fact is also evidenced by the data shown in Fig. 9(a). The same trend is observed in the effectiveness distribution along the $z/D=0$ line in Fig 9(a) where $M=2.0$ except that the local maximum occurs earlier, at about $x/D=12$. Because the injectant with $M=2.0$ has strong lateral momentum and is faster than that with $M=1.0$, it reaches the $z/D=0$ line earlier that that with $M=1.0$.

Figure 8(a) shows that, along the $z/D=1$ line, a local peak at $M=1.0$ appears at about $x/D=4$, which occurs earlier than at $M=0.5$ (see Fig. 7 (a)), because of the same reason mentioned above that the injectant originated from the hole at $z/D=0$ reaches earlier when $M=1.0$. Then,

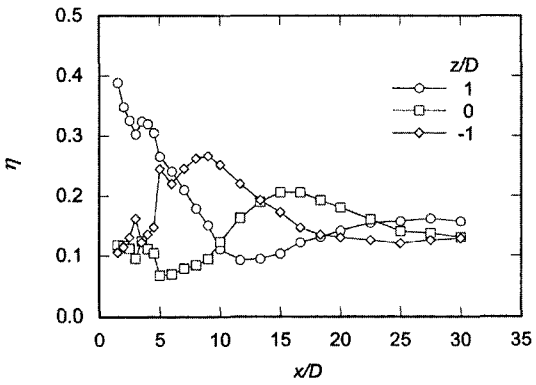

(a) Streamwise distribution

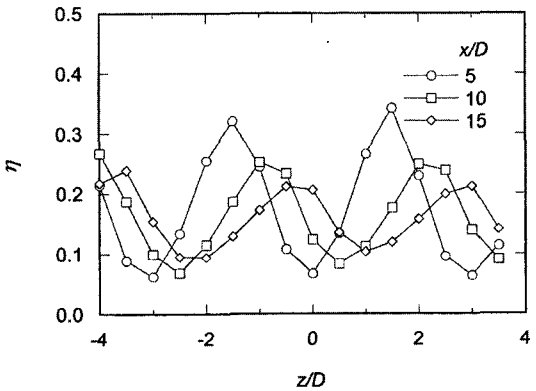

(b) Spanwise distribution

Fig. 8 Local film cooling effectiveness at $M=1.0$

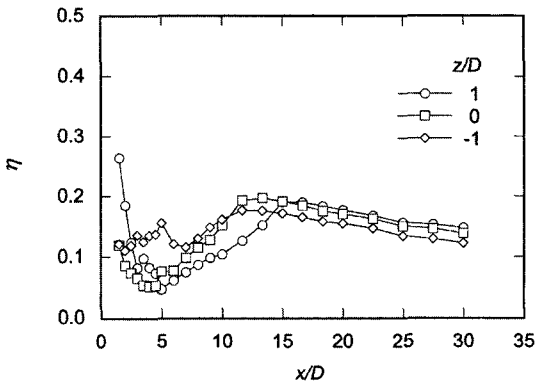

(a) Streamwise distribution

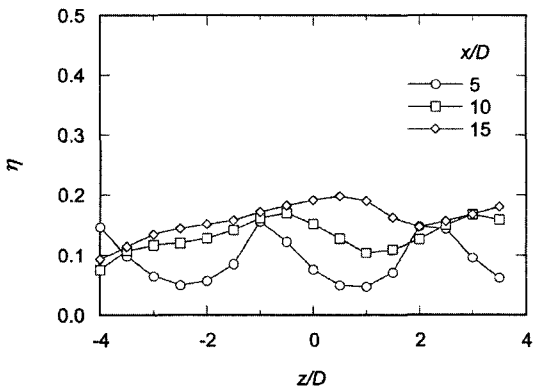

(b) Spanwise distribution

Fig. 9 Local film cooling effectiveness at $M=2.0$

the effectiveness decreases quite rapidly up to about $x/D=12$ and increases thereafter until it reaches the second local maximum at about $x/D=27$, The second local peak is caused because the injectant originated from the hole at $z/D=-3$ has reached $z/D=1$. When $M=2.0$ (Fig. 9 (a)), the maximum occurs near the injectant exit. This means that the injectant from $z/D=0$ passes through $z/D=1$ right after it is injected because it has much stronger lateral momentum compared to the case of $M=0.5$ or 1.0. At $M=2.0$, a local maximum occurs at about $x/D=12$ (which occurs at about $x/D=27$ when $M=1.0$). This is because the injectant from $z/D=-3$ has already reached $z/D=1$. Along the $z/D=-1$ line, local peaks occurs at both $M=1.0$ and 2.0 in the downstream region due to the deflection of the injectants originated from $z/D=-3$.

The effectiveness values are, in general, higher regardless of streamwise location when the mass flux ratios are lower. This is because, as can be seen from Figs. 3 and 5, the injectants are well attached to the wall when the mass flux ratios are lower. Figure 8(b) shows spanwise distribution of the film cooling effectiveness at downstream locations of $x/D=5$, 10 and 15. Compared with the data shown in Fig. 7(b), the effectiveness values are significantly reduced but the spanwise uniformity is getting better, that is, the differences between effectiveness values of maximum and minimum is getting smaller, partly because of the stronger induced flow between adjacent injectants as shown in Fig. 4. The effect of this induced flow is clearly seen in Fig. 9(b), which corresponds to $M=2.0$. The flow induction near the surface between adjacent injectants is much stronger at $M=2.0$ (see Fig. 5) and hence the uniformity is improved in spite of effectiveness values.

3.3 Heat transfer coefficient

As a baseline survey, the heat transfer coefficient with no film cooling, h_0, is measured and compared with well-known heat transfer correlation of turbulent boundary layer flow (Kays and Crawford, 1993). Figure 10 shows the streamwise variation of the heat transfer coefficient, which

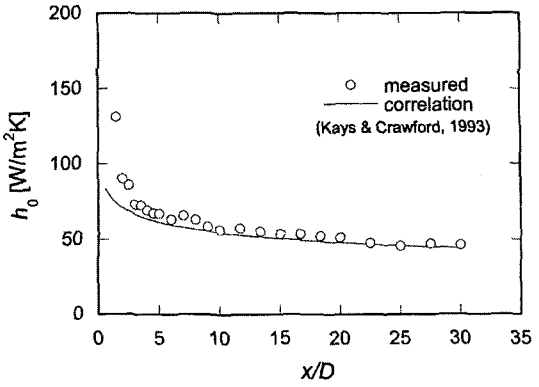

Fig. 10 Streamwise variation of local heat transfer coefficient with no injection

shows a good agreement with the correlation.

Figure 11 shows the spanwise heat transfer coefficient distribution, h_f/h_0, for the mass flux ratios of $M=0.5$, 1.0 and 2.0 at three streamwise locations of $x/D=5$, 10 and 15. When $M=2.0$, the heat transfer coefficient is largest and shows fairly uniform distribution at $x/D=5$ (see Fig. 11 (a)) because of strong secondary flow induced between adjacent injectants as shown in Fig. 6 (a). Comparing to the film cooling effectiveness data in Fig. 9(b), where the effectiveness shows wavy distribution, the induced secondary flow between adjacent injectants has more influence on the heat transfer coefficient than on the effectiveness. In the downstream region, the heat transfer coefficient shows wavy distribution, as does the effectiveness. The regions where the maximum heat transfer rate occurs are coincident with the downward flow of the vortex (see Fig. 6 (b)).

When $M=1.0$, the heat transfer coefficient shows wavy distribution at $x/D=5$ and the locations of local peaks coincide approximately with injectant locations as shown in Fig. 3(a). This different behavior from that of $M=2.0$ is due to the weaker secondary flow between adjacent injectants (see Fig. 4(a)). In the downstream region, the heat transfer coefficient shows the same pattern except that the local peaks are shifted to the right as the injectant trajectories moves to the right.

At $M=0.5$, the heat transfer coefficient dis-

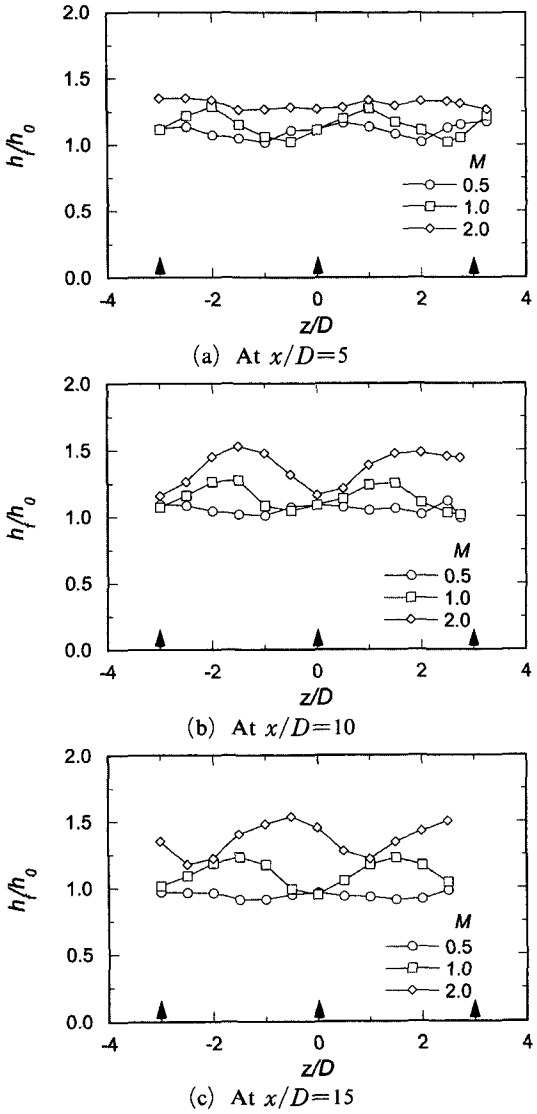

(a) At $x/D=5$

(b) At $x/D=10$

(c) At $x/D=15$

Fig. 11 Spanwise distribution of local heat transfer coefficient

tribution shows a weak wavy behavior at $x/D=5$, and is becoming more uniform in the spanwise distance as moving downstream. This is because the injectant momentum is so weak that the injectant has rapidly mixed out to mainstream.

4. Conclusions

Experimental results are presented which describe film cooling performance and heat transfer characteristics of the film coolant injected from a row of five holes with compound angle orientation of 35° inclination angle and 45° orientation angle. The mass flux ratios investigated are 0.5, 1.0 and 2.0. Some important observations are noticed and summarized below.

(1) Flow entrainment is observed between the vortices generated by adjacent injectants. The injectant with compound angle orientation entrains not only the mainstream boundary layer flow but also the adjacent injectant. The injectant with compound angle injection is characterized by a single vortex while two bound vortices are usually observed for the injectant with simple angle orientation.

(2) The effect of the mass flux ratio appears to be much more important when injected with compound angle orientation than when injected with simple angle orientation. The strength of the secondary flow induced between adjacent injectants depends on the mass flux ratio, which shows significant influence on the film cooling effectiveness and heat transfer coefficient.

(3) Along the $z/D=0$ line, the effectiveness distribution at $M=1.0$ shows strikingly different behavior from that at $M=0.5$. The effectiveness is much lower near the exit compared to that at $M=0.5$ because the injectant has such strong lateral momentum that it is deflected and deviated from the $z/D=0$ line immediately after it is injected.

(4) When $M=2.0$, the heat transfer coefficient is largest and shows fairly uniform distribution at $x/D=5$ because of strong secondary flow induced between adjacent injectant holes. Comparing with the wavy film cooling effectiveness distribution, it can be seen that the induced secondary flow has more influence on the heat transfer coefficient than on the effectiveness.

References

Ahn, J., Jung, I. S. and Lee, J. S., 2001a, "Film Cooling from Two Rows of Holes with Opposite Orientation Angles (I): Configuration Effect," *Transactions of KSME B*, Vol. 25, pp. 1122~1130.

Ahn, J., Jung, I. S. and Lee, J. S., 2001b, "Film

Cooling from Two Rows of Holes with Opposite Orientation Angles (II): Blowing Ratio Effect," *Transactions of KSME B*, Vol. 25, pp. 1131~1139.

Eckert, E. R. G., 1984, "Analysis of the Thermal Characteristics of Heated Turbulent Jets in crossflow," *ASME Journal of Engineering for Gas Turbines and Power*, Vol. 106, pp. 206~213.

Ekkad, S. V., Zapata, D. and Han, J. C., 1997a, "Heat Transfer Coefficients over a Flat-Surface with Air and CO_2 Injection through Compound Angle Holes using a Transient Liquid Crystal Image Method," *ASME Journal of Turbomachinery*, Vol. 119, pp. 580~586.

Ekkad, S. V., Zapata, D. and Han, J. C., 1997b. "Film Effectiveness over a Flat-Surface with Air and CO_2 Injection through Compound Angle Holes using a Transient Liquid Crystal Image Method," *ASME Journal of Turbomachinery*, Vol. 119, pp. 587~592.

Honami, S., Shizawa, T. and Uchiyama, A., 1994. "Behavior of the Laterally Injected Jet in Film Cooling: Measurements of Surface Temperature and Velocity/Temperature Fields within the Jet," *ASME Journal of Turbomachinery*, Vol. 116, pp. 106~112.

Kays, W. M. and Crawford, M. E., 1993, *Convective Heat and Mass Transfer*, 3rd ed., McGraw-Hill, p. 281.

Lee, S. W., Kim, Y. B. and Lee, J. S., 1995. "Flow Characteristics and Aerodynamic Losses of Film-Cooling Jets with Compound Angle Orientations," *ASME Journal of Turbomachinery*, Vol. 119, pp. 310~319.

Ligrani, P. M., Ciriello, S. and Bishop, D. T., 1992. "Heat Transfer, Adiabatic Effectiveness and Injectant Distributions of a Single Row and Two Staggered Rows of Compound Angle Film-Cooling Holes," *ASME Journal of Heat Transfer*, Vol. 114, pp. 687~701.

Ligrani, P. M. and Lee, J. S., 1996a. "Film Cooling from Two Staggered Rows of Compound Angle Holes at High Blowing Ratios," *International Journal of Rotating Machinery*, Vol. 2, pp. 201~208.

Ligrani, P. M. and Lee, J. S., 1996b. "Film Cooling from a Single Row of Compound Angle Holes at High Blowing Ratios," *International Journal of Rotating Machinery*, Vol. 2, pp. 259~267.

Ligrani, P. M., Wiegle, J. M., Ciriello, S. and Jackson, S. M., 1994a "Film-Cooling From Holes with Compound Angle Orientaion: Part 1-Results Downstream of Two Staggered Rows of Holes with 3d Spanwise Spacing," *ASME Journal of Heat Transfer*, Vol. 116, pp. 341~352.

Ligrani, P. M., Wiegle, J. M. and Jackson, S. M., 1994b. "Film-Cooling from Holes with Compound Angle Orientaion: Part 2-Results Downstream of a Single Row of Holes with 6d Spanwise Spacing," *ASME Journal of Heat Transfer*, Vol. 116, pp. 353~362.

Mick, W. J. and Mayle, R. E., 1988. "Stagnation Film Cooling and Heat Transfer Including its Effects within the Hole Pattern," *ASME Journal of Turbomachinery*, Vol. 110, pp. 66~72.

Schmidt, D. L., Sen, B. and Bogard, D. G., 1996. "Film Cooling With Compound Angle Holes: Adiabatic Effectiveness," *ASME Journal of Turbomachinery*, Vol. 118, pp. 807~813.

Sen, B., Schmidt, D. L. and Bogard, D. G., 1996. "Film Cooling with Compound Angle Holes: Heat Transfer," *ASME Journal of Turbomachinery*, Vol. 118, pp. 800~806.